DEVELOPMENT AND VALIDATION OF A FAST MID-FIDELITY COMPREHENSIVE ANALYSIS TOOL FOR GENERIC E-VTOL CONFIGURATIONS

Murat Şenipek, murat.senipek@metu.edu.tr, PhD. Candidate,
Osman Güngör, osman.gungor@metu.edu.tr, PhD. Student,
Ozan Tekinalp, tekinalp@metu.edu.tr, Professor,
Aerospace Engineering Department
Middle East Technical University (Turkey)

Abstract

This paper presents development and validation of a mid-fidelity fast vortex rotorcraft comprehensive analysis tool specialized for flight mechanics and handling quality analysis of multiple rotor configurations having severe interactional aerodynamics. Mid-fidelity simulation framework includes Vortex Particle Method (VPM) accelerated by GPU and coupled with a Generic Air Vehicle Model (GAVM) which is a mathematical model for analysis of generic configurations such as propeller aircrafts, conventional and unconventional rotorcrafts, multi-rotor and tilt-rotor eVTOL configurations. This work presents the development, integration and validation stages for a mid-fidelity aerodynamics and flight mechanics comprehensive analysis framework for further research specialized for eVTOL design, performance, control design and handling quality analysis by modeling correct rotor wake dynamics and interactions. Simulation cases are presented including rotor-rotor, rotor-body and rotor-lifting surfaces interactions for conventional helicopter and multi-rotor configurations. In addition to the development and integration, several validation cases are presented that are covering rotor in hover, rotor in edgewise flight, propeller in axial flight and rotor-body interactions. Detailed comparisons with direct CFD solutions are presented.

1. INTRODUCTION

Advances in the electric propulsion technology leads the aerospace companies and start-ups to design modern electric powered VTOL aircraft to boost the modern era city transportation. Several modern designs are developed in the last decade not only from established VTOL manufacturers such as Bell and Airbus Helicopters, but from newcomers such as Joby Aviation and Hyundai Motor Company among many others [1]. One of the most significant advantages of electric propulsion is the elimination of the need for transmission and power-train systems. Therefore, utilization of multiple rotors became more feasible than conventional engine, transmission and power-train systems. Fly-by-wire flight controls combined with multiple electric motors and control surfaces have significant advantage in terms of redundancy and handling qualities.

Several different configurations are emerged as a result of the advancements in electric propulsion ranging from multicopters (such as Volocity or CityAirbus), to tiltrotors (Bell Nexus and A^3 Vahana), to entirely new configurations [1][2]. Due to distributed propulsion and transition mechanics, these configurations tend to have significant rotor-rotor and rotor-airframe interactions than conventional type helicopters. Representing those configurations by conventional dynamic inflow models may not be sufficiently accurate [3][4]. In these conventional models, interactions are modeled by empirical factors scaled with the inflow and is not sufficient to analyze blade vortex interactions. Therefore, higher fidelity aerodynamic methods are required to generate simulation models that represent rotor wake and aerodynamic interactions to investigate aerodynamic performance, loads, handling qualities and even rotor noise [2].

Higher fidelity aerodynamic models such as vortex methods and CFD are not preferred for conceptual design, control design and flight dynamics simulations since they require high computation power. Instead of direct high-fidelity analysis, system identification and linearized inflow models are preferred for modern rotorcraft configurations [2]. However, advancements in graphical processing unit (GPU) computing technology and various development environments, some high-fidelity methods became much more efficient than before. One of the best examples is the Viscous Vortex

Particle Method (VVPM) that is inherently suitable for GPU programming to reduce the computation cost significantly. VVPM solves Navier-Stokes equations in vorticity form by using Lagrangian approach. Vortex particles are released from the aerodynamic surfaces such as rotor blades and wings to generate vorticity field in the domain of interest. Since VVPM solves Navier-Stokes equations, vortex wake dynamics and viscous diffusion effects can be included. Considering VVPM as a meshless method and having GPU-compatible structure, it provides a unique opportunity to perform comprehensive analysis and even time-marching simulation to assess the wake dynamics and interference effects.

Several application of VVPM is performed recently in order to predict rotor wake dynamics and rotor-rotor interactions [5][6][7][8]. Furthermore, coupling this methodology with rotorcraft simulation tools enable the designer to investigate aircraft flight chracteristics by including the effects of rotor wake dynamics such as wake contraction, distortion and blade vortex interactions. Implementation of VVPM brings the ability to observe the change of flow variables in any point in the domain of interest. Therefore, rotor airframe interactions can be calculated quickly with certain assumptions. Unsteady 3-D panel methods and distributed interference models may be used to couple airframe and wings aerodynamics with the wake of rotors in a flight dynamics simulation environment.

Integrating both VVPM and rotorcraft dynamics composes a high-fidelity analysis environment that can be used to perform conceptual/preliminary design and to investigate aerodynamic performance, loads and handling qualities including the effect of VVPM based rotor-rotor and rotor-airframe interactions. Since recent eVTOL configurations in design and flight-testing stages include coaxial, coaxial compound, tilt-rotor, multi-rotor, and augmented lift concepts that include severe rotor-rotor and rotor-airframe aerodynamic interactions, proposed simulation environment may easily be used to predict handling qualities and optimize the control design as well as the design itself. In this paper, all validation and simulation cases are modeled by using inviscid vortex particle method that is called as VPM.

2. VPM COUPLED ROTORCRAFT ANALYSIS

In this part, coupling of VPM with a generic air vehicle model for rotorcraft design and analysis is summarized.

2.1. Generic Air Vehicle Model

The Generic Air Vehicle Model (GAVM) is developed to perform quick analysis and simulations of a generic rotorcraft configurations [9]. GAVM is a validated multi-disciplinary, object-oriented and generic modeling and simulation tool for different air vehicles [9][10]. GAVM is coded in C++ environment as both console application and shared library. Conventional propeller airplanes, conventional and modern helicopters such as compound and tilt-rotors can be modeled and simulated. It includes generic sub-components such as rotor, wing and fuselage that form aircraft. GAVM rotor component includes rigid blade with non-uniform chord, sweep, twist distributions and two dimensional viscous, compressible airfoil aerodynamic databases. Mathematical model of rotor incorporates rigid blade element formulation that includes finite state dynamic inflow models proposed by Pitt [3], Pitt and Peters [4], and blade airloads calculations are performed by 2-D viscous airfoil data. Empirical models are integrated to simulate the effects of tip losses, blade sweep, stall-delay due to rotation, and yawed flow [11]. Rotor dynamics model provides second order coupled flapping and lagging dynamics, which includes blade inertial properties, hinge offset, and root cut out, dampers and springs [12]. Effects of inertial, Coriolis, centrifugal, and gyroscopic forces are included in the equations of rotor dynamics. Wing and body models include classical table-lookup methodology for 6-DoF airloads calculations. Modified second order lifting line theory including viscous airfoil data is optional for wings [13][14]. Generic trim algorithm implemented in GAVM software provides the equilibrium condition for a flight condition by using a gradient based constrained minimization algorithm. Rotor dynamics, variable RPM, dynamic tilt and cant options is available. Moreover, shared library version of the code enables the time-marching flight dynamics simulation of the rotorcraft.

2.2. Viscous Vortex Particle Method

Viscous vortex particle method included in this paper is based on the work done by Yücekayali [15]. VVPM is a Lagrangian Navier-Stokes (in vorticity transport form) solver based on first principles and it preserves coherent vortex structures for long distances and do not have any ad-hoc modeling parameters. Vorticity particles are generated from trailing edges of rotor blades and are convected into domain. Calculation of induced velocity is efficient and it inherently includes rotor-rotor interactions. All of these inherent advantages make the vortex particle method a natural candidate to solve the vorticity dominated incompressible flow-field around rotorcraft configurations [7]. In this work, inviscid vortex particle method is used in validation and simulation cases that only solves explicit convection part of the governing equation.

$$\frac{d\vec{x}_i}{dt} = \vec{u}_i = -\sum_{j=1}^{N} \frac{1}{\sigma_{ij}^3} K(\rho)(\vec{x}_i - \vec{x}_j) \times \vec{\alpha}_j$$

Solving above equation requires the induced contributions from all the particles to calculate the

induced velocity of a particle $\vec{u}_i$ that makes the VPM traditional N-body problem [5].

Full rotor dynamics routines are preserved in GAVM during the integration of VVPM. Only the inflow dynamics part is updated with VVPM. Several additions are implemented and algorithm is coded in CUDA C++ environment. Since the theory of vortex particle method is an n-body problem, induced velocity of each particle is calculated for all other particles as an explicit solution for a given time step. Therefore, it is very feasible to implement it in a GPU environment for parallelization. Implementation of GPU algorithm in CUDA reduces the solution time from 9 hours to 5 minutes for a desktop computer. Generic Newton-Raphson based trim algorithm is implemented that uses finite state rotor models to find the trim initially, then time marching full helicopter trim is initiated to find the trim condition by including all the rotor dynamics, vehicle and wake dynamics, interference effects coming from the VVPM. Time marching trim algorithm uses the identical finite-state Jacobian for VVPM full helicopter trim with moving average filter for oscillatory loads. For some high-speed cases, filter creates lag in the dynamics, which requires lower relaxation factor. Generic trim algorithm is applicable to multiple rotor configurations including RPM variation and rotor tilting as provided in Figure 1.

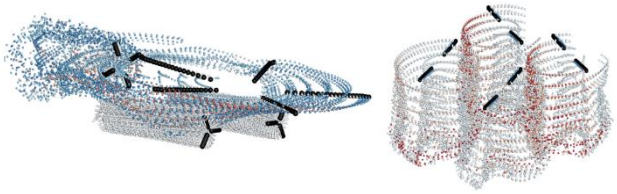

Figure 1 Generic compound helicopter and multi-rotor VVPM solutions in trim

One of the biggest problems in VPM based methods is the collocation of far particles. Their effects on the rotor becomes negligibly small; however, they are staying and going into calculations. Since the computation complexity is $O(n^2)$, they affect the computational cost negatively. There are some methods applied for similar problems such as wake trimming [16] and Fast-Multipole Methods (FMM) [7]. FMM is one of the best algorithms, which uses a scalar function for the particles far away. It uses Octree data structure to discretize the domain.

In this work, octree discretization is utilized in spatial coordinates to merge vorticity of the close particles that satisfy the rule proposed by Spalart as illustrated in Figure 2 [7].

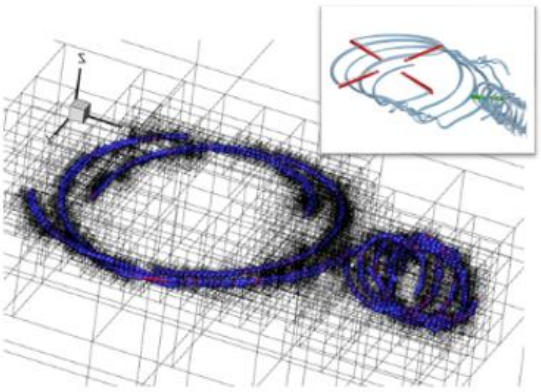

Figure 2 Octree discretization of a convenctional helicopter VVPM wake

The rule states that if two vortex particles are close enough and have an angle smaller than χ_0, they can be merged into a single vortex structure. This criterion is set to limit the particle merging of two particles nearly opposite vorticity. Therefore, far wake particles (when their age becomes larger than a predefined threshold) are merged for a desired resolution and total number of particles are reduced.

Since octree algorithm discretizes the domain into cubic cells, it can be used to generate volume and surface meshes for post-processing purposes. This algorithm enables the user to visualize the flow properties without generating extra mesh. Defining the size of the minimum cell provides an adaptive mesh for a given time during the solution as illustrated in Figure 3. Furthermore, implementation of Octree prepares a baseline for further FMM algorithm implementations.

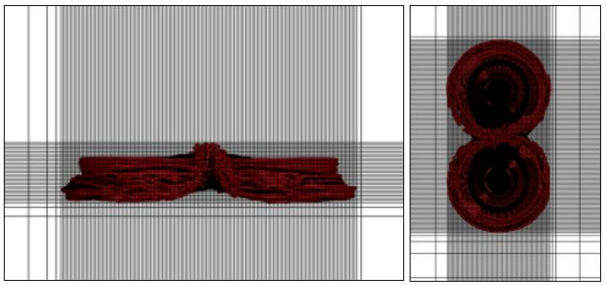

Figure 3 Two side view of octree cartesian mesh

2.3. VPM – Body Interaction Model

Comprehensive analysis tools such as CAMRAD, CHARM and FLIGHTLAB implements rotor body interactions as point body 6-DoF aerodynamic database for α and β envelope as given in Figure 4 [17][18][19].

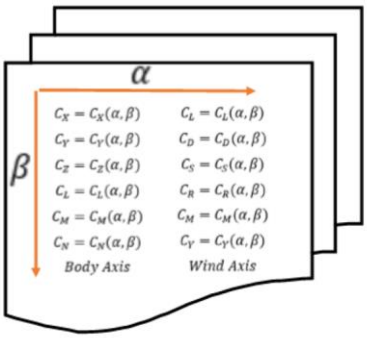

Figure 4 6-DoF Point aerodynamic database

In some cases, without integrating in the trim or simulation model, 3-D unsteady panel method coupled with rotor wake. For higher fidelity analyses, these tools provide CFD coupling interfaces.

GAVM-VVPM provides both point body and distributed pressure interaction models for rotor-body interactions. Point body models may be useful for small and aerodynamic components such as horizontal stabilizer and vertical fin in main rotor wake. However, rotor fuselage interactions may not be accurately modeled by point body interaction model. Since 3-D unsteady panel method brings computational complexity, a simple distributed pressure interaction model is developed and implemented in GAVM. Distributed pressure model requires previously generated CFD pressure database for fuselage for a proper envelope all angle of attack and sideslip angles. This database will form a 3-Dimensional dataset (α, β, C_p) to be used by the VPM wake for each cell as illustrated in Figure 5.

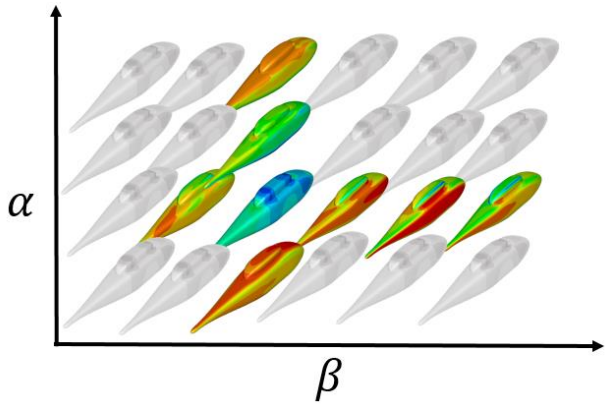

Figure 5 Illustration of pressure databases for all wind envelope

Since GPU based VPM algorithm can calculate airspeed at any given location, all cell locations are input as velocity calculation points and local pressure is interpolated as a function of angle of attack and beta as illustrated in Figure 6.

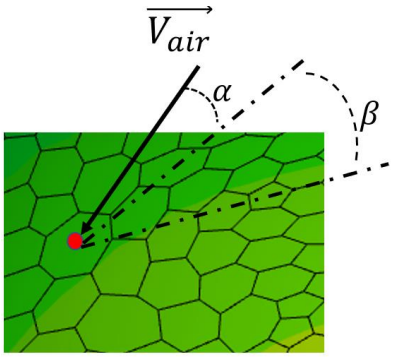

Figure 6 Air velocity and wind angles on surface cells

It is a similar approach for 3-D panel method since it also uses the same velocity field and tries to satisfy zero normal velocity. In this approach, previously generated viscous aerodynamic database is utilized and coupled with VPM. Methodology has similar assumptions with widely used point-body aerodynamic models but provides better resolution and is continuously being validated against available data. The main deficiency of the method is that it does not affect the flowfield and does not produce vorticity from the sharp edges. Only one-way interaction is available.In addition, GAVM-VVPM tool enables to investigate the effects of interactions by simply turning on/off for all rotor-rotor, rotor-body interactions. When the interactions are deactivated, each component is solved as an isolated body. In that case, distributed pressure solutions provide identical forces and moments for a point body model for the fuselage.

In conclusion, distributed pressure database is being optimized and being validated for available data. Since it can be easily integrated in GPU architecture, mid-fidelity simulations are available for full interaction analysis.

3. CFD MODELLING FOR VALIDATION

ROBIN wind tunnel test cases are modelled with CFD approach in order to compare flow structures [21]. Commercial CFD package StarCCM+ is utilized in CFD simulations. Density based RANS solver with implicit unsteady time stepping is coupled with Spalart-Allmaras turbulence model. Curvature correction is activated. Time step is defined such that 1-degree advancement in azimuth is achieved for rotor rotation. Second order scheme is used for time discretization with 10 inner iterations. Spatial discretization scheme for both flow and turbulence is second order upwind scheme. Roe's flux splitting scheme is used for inviscid flux calculations.

In order to provide degree of freedoms for rotor motion, overset-meshing technique is utilized. A subdomain with polyhedral surface and volume elements is generated for each blade. Cartesian mesh is used in the background domain. A refinement

region inclosing the blades is utilized in the background mesh and extended over the rotor wake. Figure 7 shows background mesh cutout, ROBIN body surface mesh and blade-background overset mesh interface.

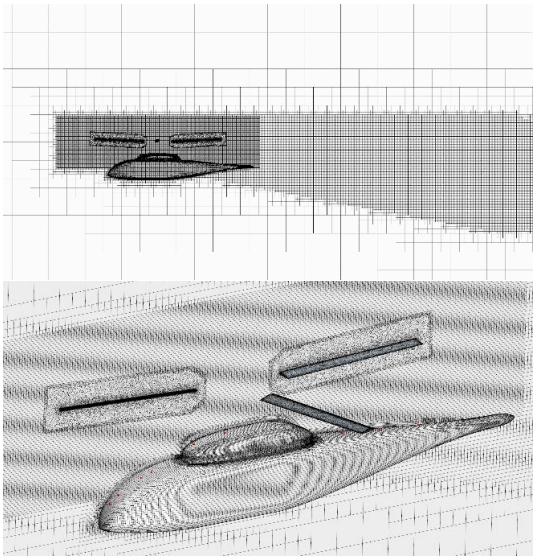

Figure 7 CFD Model Solution Domain, Background Mesh, ROBIN Body and Blades

For ROBIN body and rotor blades, 10 prism layers satisfying wall function condition are generated. Each blade domain consists of nearly 1 million polyhedral elements. Background domain mesh is resulted in 12 million hexahedral elements. Total number of elements sums up to 16 million.

Rotor trim approach employed in the wind tunnel tests of ROBIN is replicated in the CFD model. Rotor is trimmed to target thrust and first harmonics of the flapping motion are trimmed to zero. The details of the rotor trim and blade motion are provided in a previous work [20].

4. VALIDATION AND SIMULATION CASES

In this chapter, available validation cases are provided for isolated rotors in hover, edgewise flight and axial flight. Robin rotor-body interaction case is modeled with both inviscid VPM and CFD to compare the rotor-body interactions and rotor wake. Surface pressure contours, unsteady pressure values, wake geometry, flowfield velocity distribution and BVI conditions are compared and investigated. Furthermore, rotor-rotor interaction cases, full helicopter and multi-rotor sample analyses cases are presented in appendix to show the capabilities.

4.1. S-76 Hover and Forward Flight Case

S-76 helicopter main rotor aerodynamic and performance validation model is generated as blade properties are summarized in Table 1. Blade planform, airfoil and twist distribution are given in Figure 8. Hover tests are performed in 1000 hp whirl tower test stand in Sikorsky for different thrust settings [23].

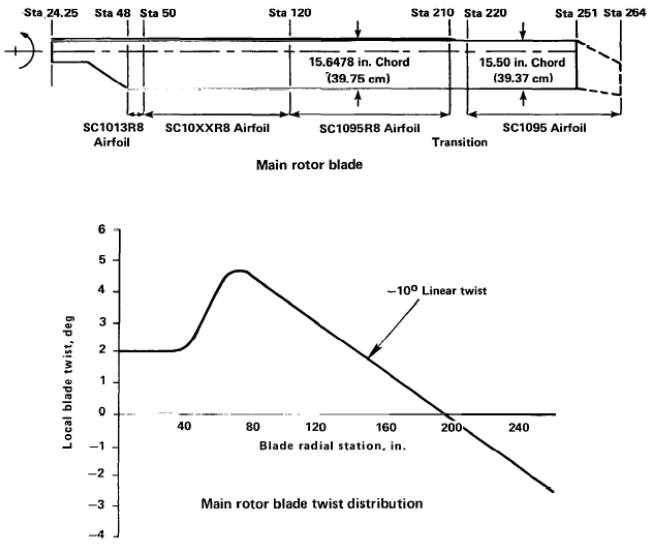

Figure 8 S-76 Blade Planform

Table 1 S-76 Main Rotor Specifications

Main Rotor Parameters	
Radius [m]	6.7
Nominal Chord [cm]	39
Solidity	0.0748
\# of blades	4
Airfoils	SC1095 & SC1095R8
Flapping Hinge Offset	3.79 %
Lock Number	11.6
RPM	293
Tip Speed [ft/s]	675

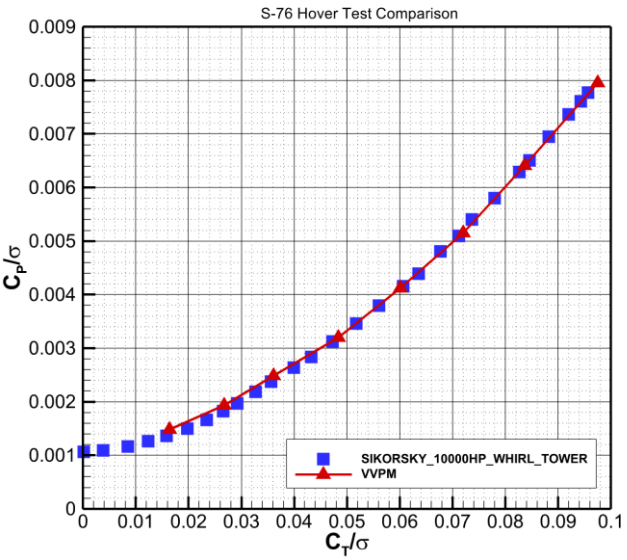

Figure 9 Power and Thrust Coefficient Comparison

In Figure 9, good correlation is obtained with the isolated rotor simulation case and the experimental data. For all thrust settings, simulation results are sufficiently close to the experimental data. Furthermore, velocity field together with vortex particles are illustrated in Figure 10. Vorticity contours are plotted for vertical plane and tip vortices can be clearly seen in Figure 11. Note that all post process visuals are produced by automated octree algorithm.

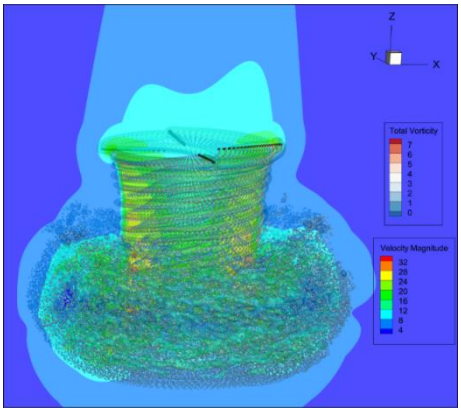

Figure 10 Vorticity Iso-Surfaces Colored by Velocity

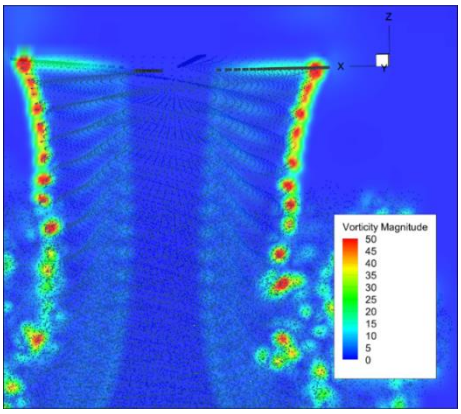

Figure 11 Vorticity contours together with particles

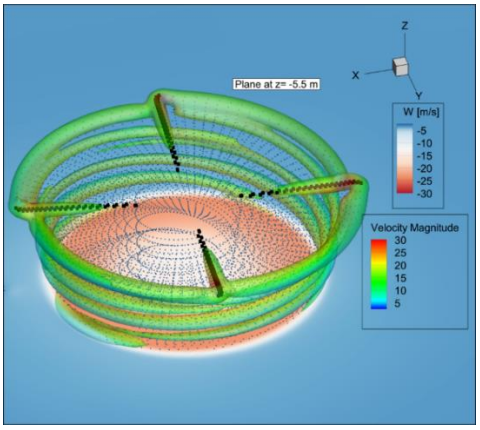

Figure 12 Vorticity isosurfaces and downwash contours at -5.5 m below the rotor disk

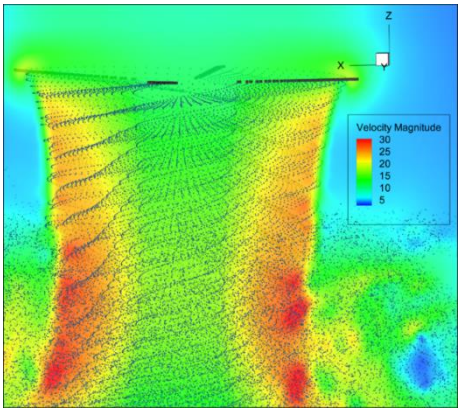

Figure 13 Velocity contours with particles for a vertical cross-section

Further details on velocity and vorticity fields are summarized in Figure 12 and Figure 13.

Forward flight analyses are conducted for different advance ratios for AMES 80x120 Wind Tunnel test conditions [24][25]. High-speed forward flight analysis solution is illustrated in Figure 14 with vortex particles, velocity contours and vorticity Iso-surfaces.

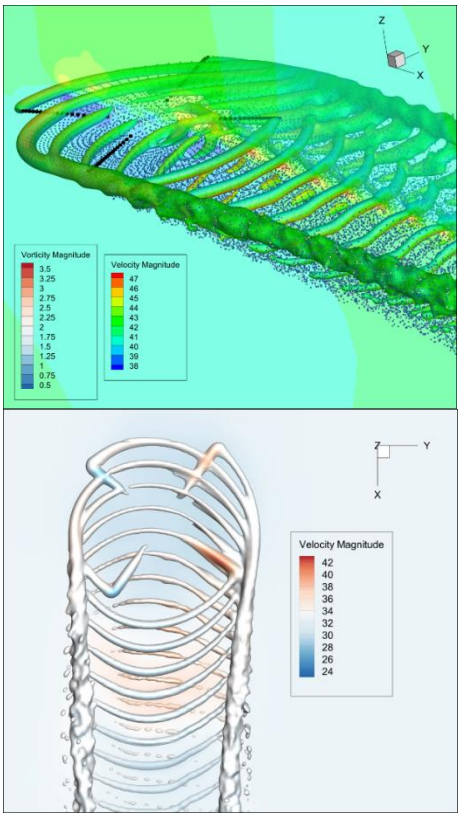

Figure 14 S-76 Rotor Forward Flight Analysis $\mu = 0.25$

VPM rotor model is trimmed to $C_T/\sigma = 0.08$ and analyzed for different shaft tilt angles α_s and different forward velocities. Analyses are performed up to 0.25 advance ratio, which corresponds to 100 knots of wind speed. Analyses show consistency in general, however; there is a slight underestimation of test

results due to tunnel effects. Results obtained for wind tunnel validation cases are plotted in Figure 16.

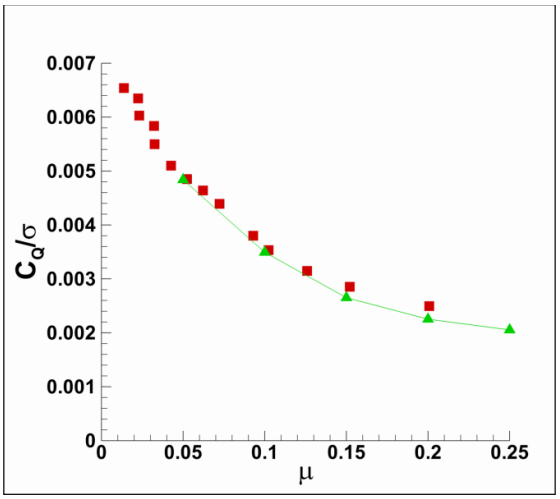

Figure 15 S-76 Wind Tunnel Power Coefficient vs. advance ratio($\alpha_s = 0°$)

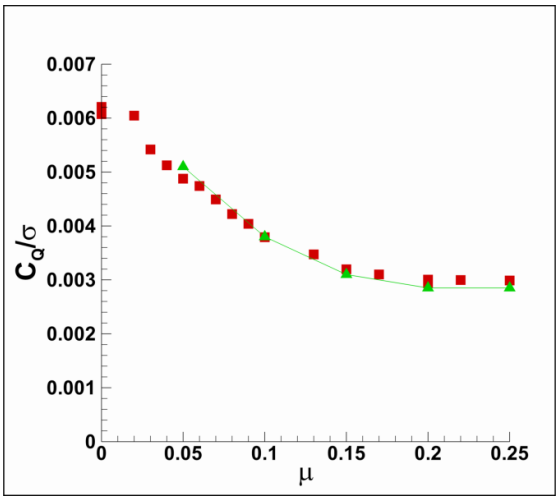

Figure 16 S-76 Wind Tunnel Power vs. Thrust Coefficient Validation ($\alpha_s = -2°$)

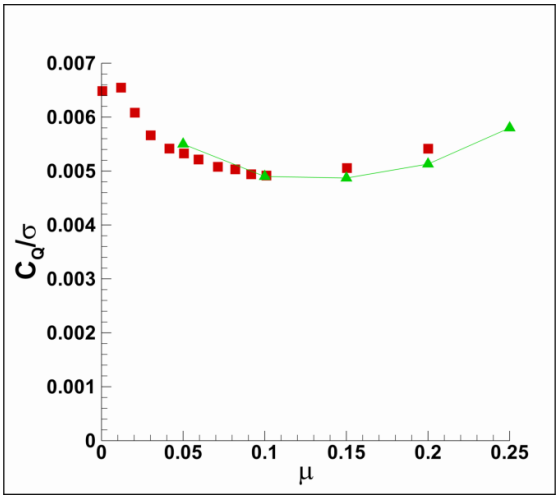

Figure 17 S-76 Wind Tunnel Power vs. Thrust Coefficient Validation ($\alpha_s = -10°$)

4.2. CLARK-Y Propeller Validation

Rotor in hover and rotor in edgewise flow validation cases are followed by rotor in axial flight cases in order to validate the propeller performance operating in cruise conditions in cruising eVTOL designs. An experimental case performed by NACA is selected for the validation [26]. In the analysis cases, propellers are tested for different axial velocities. Two bladed propeller geometry having Clark-Y airfoils are modeled as given in Figure 18 to perform VVPM analyses.

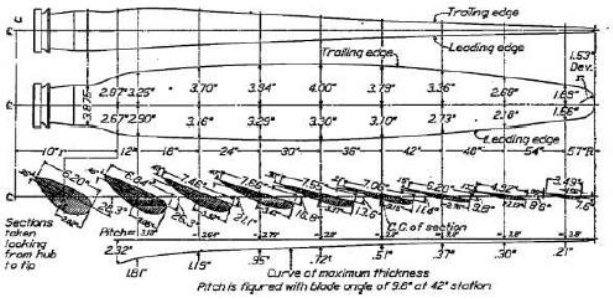

Figure 18 Clark-Y Propeller Definition

In these analyses, propeller thrust is trimmed to experimental thrust for all freestream speeds at which experiments are conducted. Vortex particles and farfield octree clustered particles and vorticity Iso-surfaces are illustrated in Figure 19 and Figure 20. In Figure 19, vortex particles at the downstream are merged with Octree algorithm, which produces a single particle having higher strength from several particles that increases the solution speed.

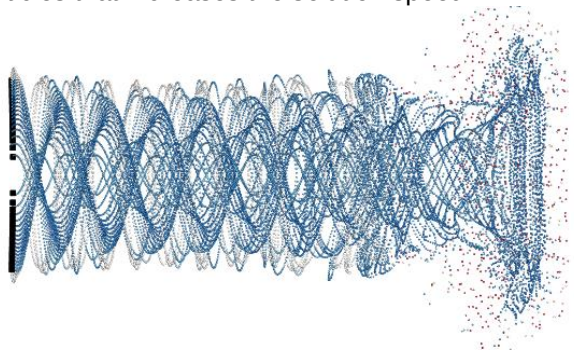

Figure 19 Vortex particles in CLARK-Y propeller case

Figure 20 illustrates high-speed axial flow solution where tip vortices and wake contraction with the help of streamlines are clearly identified.

In order to compare the results with experimental data, propellers are trimmed to experimental thrust values for each case as given in Figure 22. In Figure 21, time dependent thrust change is summarized for some analysis conditions to show the convergence of the trim algorithm.

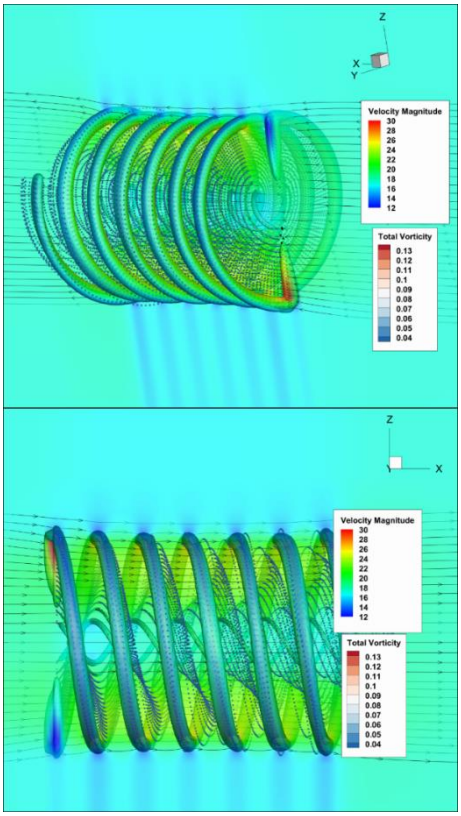

Figure 20 Vorticity isosurfaces at 50 knots axial flight case

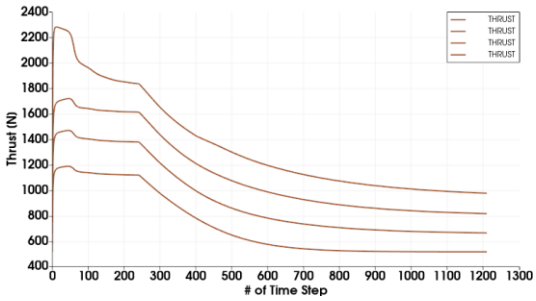

Figure 21 Thrust trim history

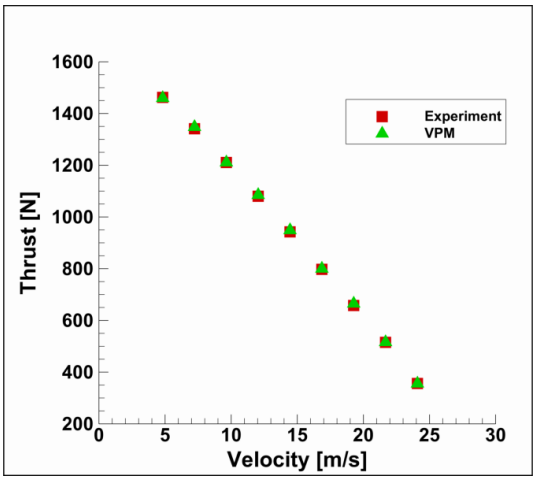

Figure 22 Propeller thrust vs. axial velocity

Resulting power values are provided in Figure 23. Thrust trimmed results show almost consistency with experimental data. Almost for all airspeed values, VPM solutions underestimates the experimental data. Higher axial flow cases are more dependent on airfoil databases. It may be concluded that the calculated drag values for 2-D airfoil databases might be slightly lower than actual drag.

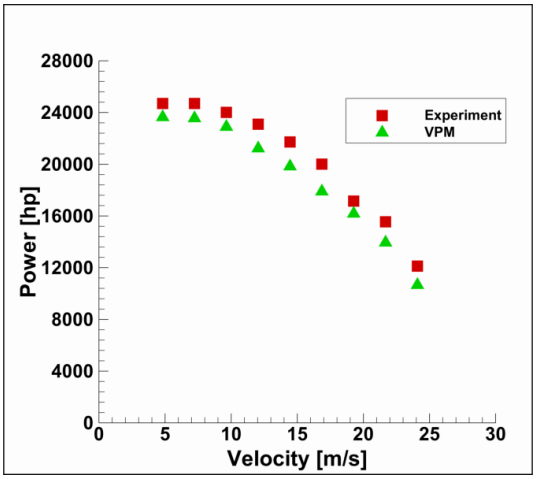

Figure 23 Propeller power vs. axial velocity

4.3. Rotor-Body Interaction (ROBIN) Case

eVTOL designs emerged in diverse configurations changing from multicopters to tilt rotors. Rotor-body interactions may be significant for some configurations. Therefore, interaction prediction capability of the presented VPM approach is investigated using famous NASA wind tunnel test campaign results, ROBIN. Test setup consists of a scaled rotor and a generic fuselage geometry as shown in Figure 24.

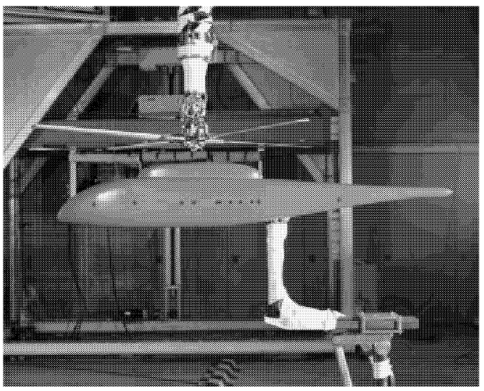

Figure 24 Rotor Body Interference configuration installed in 14-by-22 foot subsonic tunnel test section

Fuselage is instrumented with unsteady pressure sensors. Tests were performed for varying air speed and thrust conditions. A low speed and a high-speed test run are selected at single thrust condition for validation of presented VPM approach. The VPM results are also supported with CFD results to comment on flow structures and their interaction with fuselage.

Low speed test condition (μ=0.05) is selected to compare unsteady pressure fluctuations with experimental data. Test condition is analyzed for both VPM and CFD. Distributed pressure interaction model provides similar results with CFD when surface pressure contours are compared as given in Figure 25.

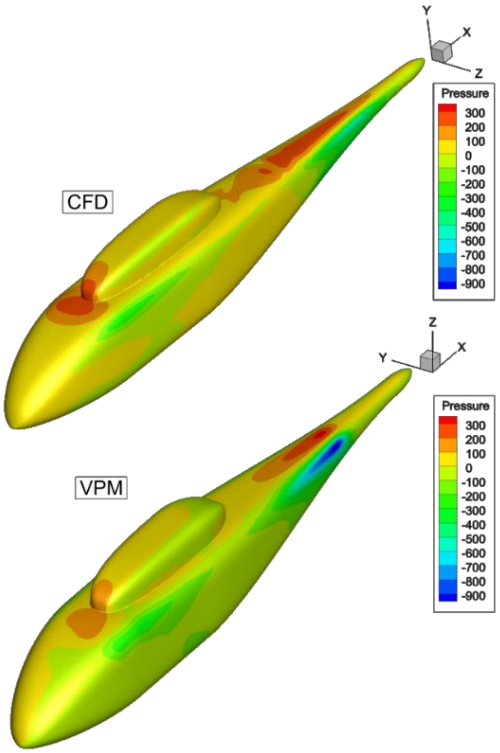

Figure 25 Pressure contours comparison for μ=0.05

In Figure 26 pressure fluctuations measured from the nose of the fuselage is compared with the test data. Both VPM and CFD results are consistent with the experimental data providing an accurate mean and peak-to-peak values for the pressure.

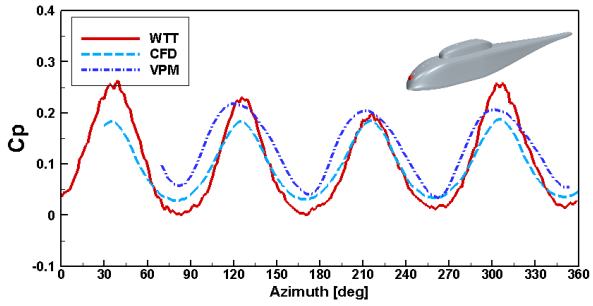

Figure 26 Unsteady Presssure Variation, Nose

Similarly, measurements from pressure sensor located on top of the tailboom cone is compared with CFD and VPM in Figure 27, which provides consistent results between CFD and VPM and slightly above the experimental data. Furthermore, peak pressure values are consistent.

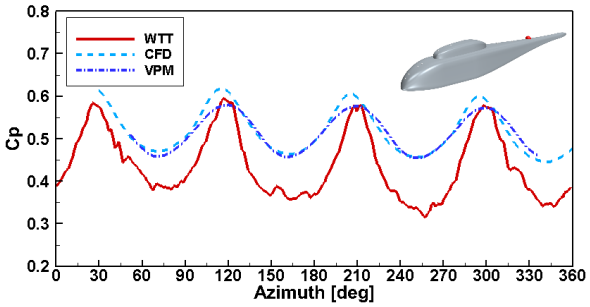

Figure 27 Unsteady Presssure Variation, Tail

The pressure data has significant 4/rev variation that is also captured by both methods. At the nose sensor, mean and peak-to-peak values of pressure variation is predicted successfully. However, at the tail boom, there is slight shift between test result and predictions for both mean and peak-to-peak values.

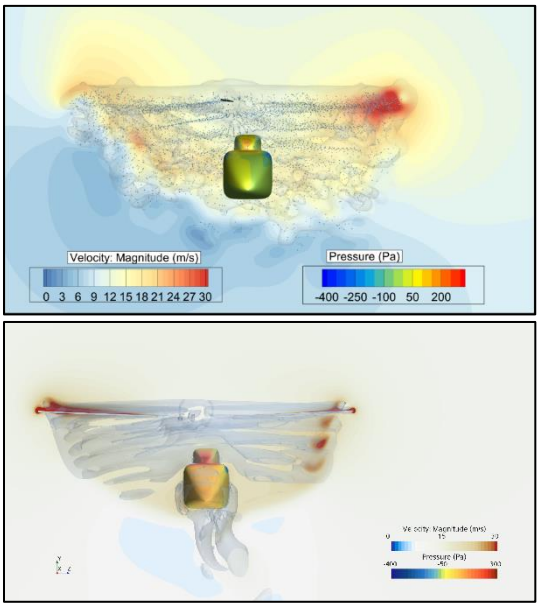

Figure 28 Vorticity isosurfaces and air velocity contours from front view (upper: VPM, lower CFD)

Wake geometries and flow properties are compared for both methods as illustrated in Figure 28, Figure 29 and Figure 30 from 3-View.

Front view represents similar wake and downwash for both methods. Advancing side of CFD result has higher induction on starboard side than VPM. However, in both cases retreating blade tip vortex has higher vorticity. In Figure 29, side view of both methods is illustrated. Wake skew angle is captured well for both methods. There is no vorticity of stagnation due to fuselage in VPM based methodology since it is a one-way interaction model. On the other hand, CFD based solution captures full body wake. Fuselage pressure contours are observed as similar.

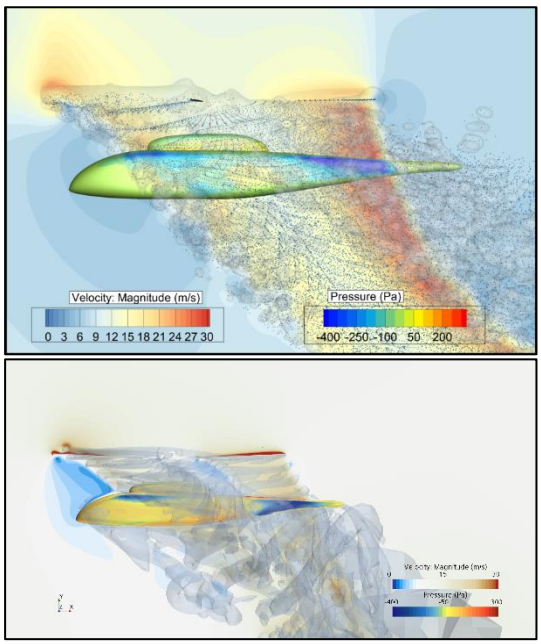

Figure 29 Vorticity isosurfaces and air velocity contours from side view (upper: VPM, lower CFD)

In Figure 30, top view isosurfaces and velocities in horizontal plane is illustrated. Due to wake skew, higher velocity regions are similar for both cases. However, rolled up tip vortices are observed stronger in CFD based solutions.

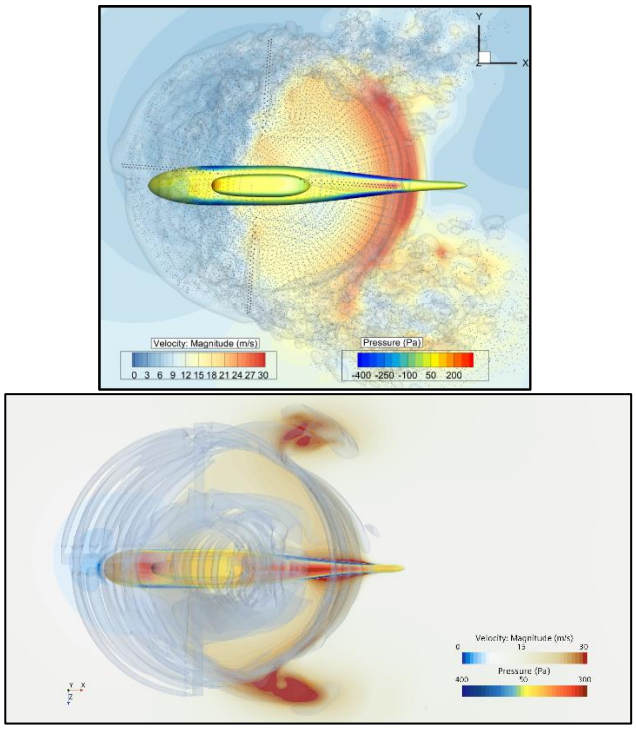

Figure 30 Vorticity isosurfaces and air velocity contours from top view (upper: VPM, lower CFD)

Another experiment case is selected to compare both models in rotor in high speed. Analyses are performed for 81 knots ($\mu = 0.231$ & $C_T/\sigma = 0.065$). In Figure 31, high speed wake comparison is performed.

Wake geometries and locations of blade vortex interactions are observed to be similar. Advancing blade interact with all other blade tip vortices in both simulations. Main critical point here is the BVI induced dynamic stall that is observed in full CFD analysis at the trailing edge about 0.8 r/R spanwise location. Separation generates extra vorticity that is convected through rotor wake. This phenomena cannot be captured by VPM since the particle generation for dynamic stall cases are not modeled yet.

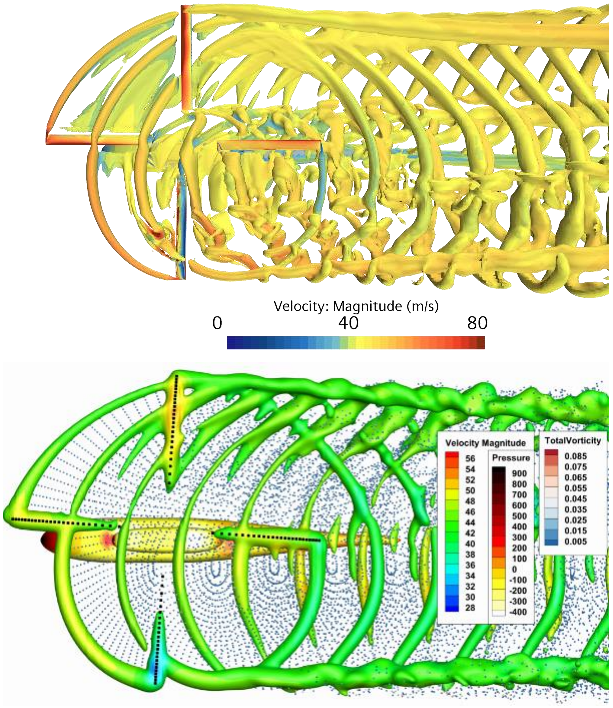

Figure 31 High speed wake comparison

Pressure fluctuations are also compared for the nose of the fuselage as given in Figure 32. CFD correlates well with the experimental data; however, VPM over predicts mean pressure and the peak-to-peak values are too small.

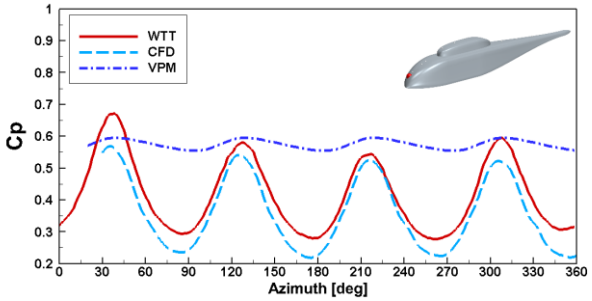

Figure 32 Pressure fluctuations at the nose

In Figure 33, advancing side blade vortex interaction is investigated in a close view. Multiple cut planes are generated to track the path and strength of the tip vortices. BVI locations and roll up structure is similar for both bases.

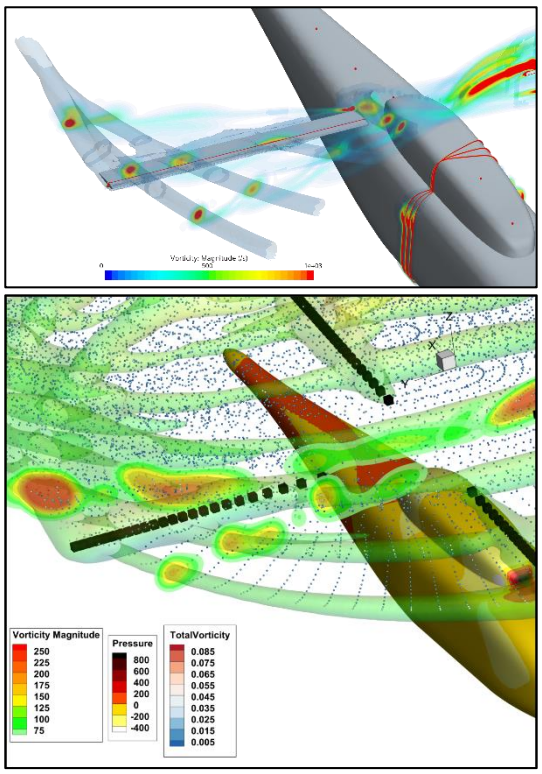

Figure 33 Advancing side BVI comparison

5. REMARKS

In this paper, development and integration of GPU accelerated VPM based flow solver with generic rotorcraft model is presented. Extensive validation and simulation cases are included ranging from isolated rotor/propeller analyses to rotor-body interactions.

VPM based solver is coupled with generic rotorcraft analysis software that brings ability to trim and simulate any rotorcraft configuration (tilt-rotors, compound helicopters, multiple rotors etc.) including full rigid coupled rotor dynamics. Architecture is suitable for design exploration, loads and control simulation analyses. Sufficient level of validation is achieved for hover, edgewise flight and axial flight.

Vortex particle methods inherently solve rotor-rotor interactions since all vorticity sources in the domain interacts with each other due to the theory of vortex particle methods. Induced velocity calculations are performed for $n \times n$ number of particles that makes the complexity of VPM $O(n^2)$. Since the formulation is explicit, it is very suitable for parallelization. In addition, since memory requirement and computation complexity are low for a given particle, it is highly applicable to GPU based computation. CUDA based acceleration reduces the computation time for a middle fidelity rotor in hover solution (100,000 particles) from 9 hours to 5 minutes and complexity becomes linear up to GPU limit and only slope changes afterwards.

Distributed pressure interference model is implemented with the VPM solver with aforementioned assumptions. CFD generated aerodynamic database is used to interpolate local pressure values on fuselage. Main motivation is to model the one-way rotor-body interactions in a suitable way for GPU based calculations to provide fast response and sufficient accuracy for future simulations. ROBIN case is modeled for validation and promising results are obtained. Applied methodology will be optimized by using different validation cases.

Future work will be focused on control design and handling quality analyses for eVTOL concepts including mid-fidelity interactions. This tool provides tight coupling interface with MATLAB Simulink to perform dynamic simulations.

Additional simulation cases are provided in Appendix to show the capabilities of VPM based generic rotorcraft model.

6. REFERENCES

[1] R. Niemiec, F. Gandhi, M. J. S. Lopez, and M. B. Tischler, “System identification and handling qualities predictions of an eVTOL urban air mobility aircraft using modern flight control methods,” *Vert. Flight Soc. 76th Annu. Forum Technol. Disp.*, 2020.

[2] Jeffrey D. Keller et. al., “Linearized Inflow and Interference Models from High Fidelity Free Wake Analysis for Modern Rotorcraft Configurations,” 2020.

[3] D. M. Pitt and D. A. Peters, “Theoretical Prediction of Dynamic-Inflow Derivatives,” *Vertica*, vol. 5, no. 1, 1981.

[4] D. A. Peters and C. J. He, “Correlation of Measured Induced Velocities with a Finite-State Wake Model,” *J. Am. Helicopter Soc.*, vol. 36, no. 3, pp. 59–70, 1991, doi: 10.4050/JAHS.36.59.

[5] J. Zhao and C. He, “A hybrid solver with combined CFD and viscous vortex particle method,” in *Annual Forum Proceedings - AHS International*, 2011, vol. 1.

[6] E. J. Alvarez and A. Ning, “Development of a vortex particle code for the modeling of wake interaction in distributed propulsion,” 2018, doi: 10.2514/6.2018-3646.

[7] J. Zhao and C. He, “A viscous vortex particle model for rotor wake and interference analysis,” *J. Am. Helicopter Soc.*, vol. 55, no. 1, 2010, doi: 10.4050/JAHS.55.012007.

[8] P. Singh and P. P. Friedmann, “A computational fluid dynamics-based viscous vortex particle method for coaxial rotor interaction calculations in hover,” *J. Am. Helicopter Soc.*, vol. 63, no. 4, 2018, doi: 10.4050/JAHS.63.042002.

[9] M. Şenipek, “Development of an Object-Oriented Design, Analysis and Simulation Software for a Generic Air Vehicle,” METU, 2017.

[10] M. Şenipek, A. Yücekayalı, and A. T. Kutay, “APPLICATION OF GENERIC AIR VEHICLE SIMULATION MODEL FOR REAL-TIME AERO-ACOUSTIC NOISE COMPUTATION OF PROPELLER AIRCRAFTS,” 2017.

[11] Z. Du and M. Selig, “A 3-D stall-delay model for horizontal axis wind turbine performance prediction,” *1998 ASME Wind Energy Symp.*, 1998, doi: 10.2514/6.1998-21.

[12] R. T. N. Chen, “Flap-lag equations of motion of rigid, articulated rotor blades with three hinge sequences,” *NASA Tech. Memo. 100023*, no. November, 1987, [Online]. Available: http://hdl.handle.net/2060/19880003113.

[13] A. Wickenheiser and E. Garcia, “Aerodynamic Modeling of Morphing Wings Using an Extended Lifting-Line Analysis,” *J. Aircr.*, vol. 44, no. 1, pp. 10–16, 2007, doi: 10.2514/1.18323.

[14] A. M. Wickenheiser and E. Garcia, “Extended Nonlinear Lifting-Line Method for Aerodynamic Modeling of Reconfigurable Aircraft,” *J. Aircr.*, vol. 48, no. 5, pp. 1812–1817, 2011, doi: 10.2514/1.c031406.

[15] A. Yücekayalı, “NOISE MINIMAL AND GREEN TRAJECTORY AND FLIGHT PROFILE OPTIMIZATION FOR HELICOPTERS,” Middle East Technical University, 2020.

[16] E. J. Alvarez, A. Ning, “High-Fidelity Modeling of Multirotor Aerodynamic Interactions for Aircraft Design”, AIAA Journal, https://doi.org/10.2514/1.J059178

[17] “FLIGHTLAB – Theory Manual 2008” www.flightlab.com

[18] W. Johnson, “CAMRAD II: Comprehensive Analytical Model of Rotorcraft Aerodynamics and Dynamics Volume I: Theory.”

[19] CHARM - Comprehensive Analytical Model of Rotorcraft Aerodynamics and Dynamics. Available http://www.continuum-dynamics.com/pr-charm.html

[20] O. Güngör, M. Şenipek, A. Ezertaş, “Computational Fluid Dynamics Simulations of S76 Rotor Wind Tunnel Tests”, 10th Ankara International Aerospace Conference, September 2019, Ankara, Turkey

[21] R.E. Mineck, S.A. Gorton, Steady and Periodic Pressure Measurements on a Generic Helicopter Fuselage Model in the Presence of a Rotor, NASA/TM-2000-210286, Langley Research Center, Hampton, Virginia

[22] P. R. Spalart, “Vortex methods for separated flows,” *NASA Tech. Memo.*, no. 100068, 1988.

[23] D. Jepson, R. Moffitt, K. Hilzinger, and J. Bissell, “Analysis and Correlation of Test Data from an Advanced Technology Rotor System,” California, 1983.

[24] W. Johnson, “Performance and Loads Data from a Wind Tunnel Test of a Full-Scale Rotor with Four Blade Tip Planforms,” California, 1980.

[25] P. M. Shinoda, “Full-scale S-76 rotor performance and loads at low speeds in the NASA Ames 80- by 120-Foot Wind Tunnel,” *NASA Tech. Rep. 110379*, vol. 1, pp. 1–248, 1996.

[26] D. H. Wood, “Full-Scale Tests of Metal Propellers at High Tip Speeds.” NACA.

7. APPENDIX

7.1. Interaction Simulations

In this part, rotor-rotor and rotor-surface interaction cases are represented. For rotor-rotor interactions, side-by-side and coaxial propeller interactions cases will be presented. Preliminary rotor-surface interaction model is integrated for a full helicopter case and results are presented. In the final paper, simulation results will be replaced by available experimental data to validate rotor-rotor and rotor-surface interactions.

7.1.1. Side-by-Side and Coaxial Rotors

In this case, sample propellers are modeled which have two bladed S-76 helicopter rotors. Side-by-side and coaxial rotors are simulated for hover and forward flight to demonstrate the effects of aerodynamic interactions. Since wake particles holds the information of parent rotor, it can easily be solved by separate VPM solution which reduces the computational cost. In Figure 34, particles of interaction on/off case between side by side propellers are shown.

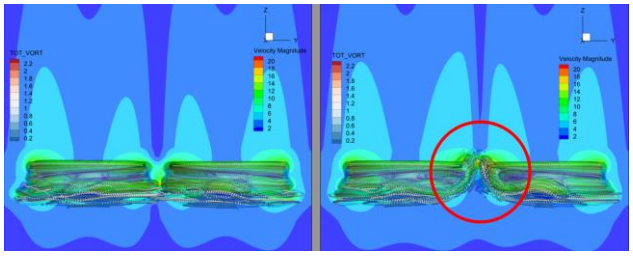

Figure 34 Coax Propellers Interactions Off/On

The distance between propellers is the main parameter of interaction. Rotor not only affects the downstream flowfield, but also affect all domain. Therefore, close proximity of rotors increases the oscillatory aerodynamic loading on blades that is critical for fatigue life of the components and aeroacoustic noise.

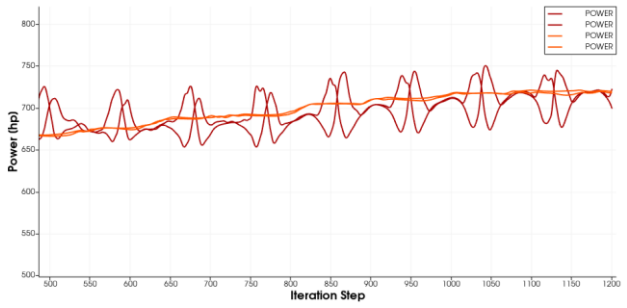

Figure 35 Power vs. Iteration step for side-by-side propellers with interactions on/off

Propeller required power is compared with interactions off case as illustrated in Figure 35. It can be observed that the peak-to-peak values of oscillatory torque are significantly increased due rotor-rotor aerodynamic interactions. Similarly, it is also possible to simulate coaxial and partially overlapping rotors with aerodynamic interactions effects as provided in Figure 36. Development of rotor wake is illustrated for 8th revolution for a coaxial configuration.

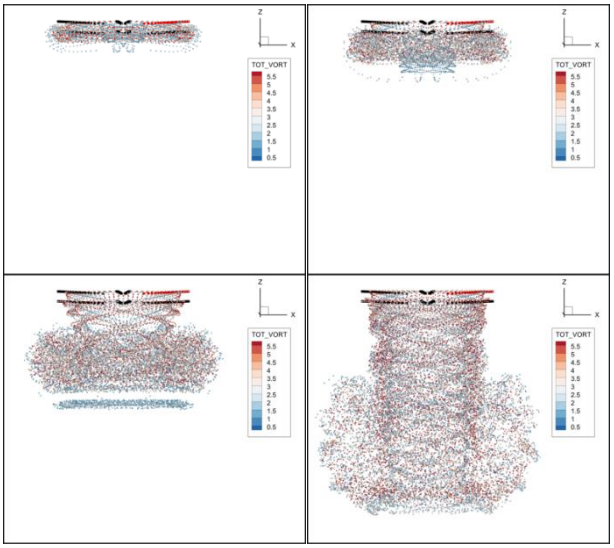

Figure 36 Coaxial rotor solution development of particles for 1st,2nd,4th and 8th revolution

Figure 37 illustrates the change of thrust levels for both rotors after including the rotor-rotor interactions. Thrust values of both rotors are affected negatively due to the other rotor's downwash. Upper rotor is affected relatively smaller as expected since the downwash velocity is relatively lower at the upstream.

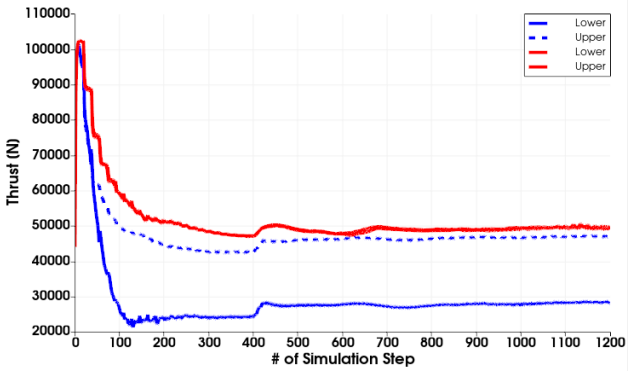

Figure 37 Comparison of individual Thrust values for both rotors with and w/o interactions

7.1.2. H/C Main Rotor Empennage Interactions

Point body interaction modeling is implemented for aerodynamic surfaces with VPM. One-way interaction is available from rotors to aerodynamic bodies. In point interaction model, aerodynamic bodies are modeled by using 6-DoF databases for a matrix of α and β values (optionally with a control input database). They can be either point fuselage, wing or

control surfaces. VPM induces rotor-induced velocities onto aerodynamic surfaces and forces and moments on the surfaces are calculated for total airspeed acting on. Therefore, time-marching total airspeed is calculated via both mathematical model and VPM rotor wake. It is the fastest model for rotor surface interaction analysis since it assumes the body as a point and calculates wake induced velocity for a single point.

Sample case is modeled for a full helicopter trim at low airspeeds where main rotor and horizontal tail interference is high. The main effect is expected to be seen on body pitch angle since downwash on horizontal stabilizer produces extra pitch-up moment on the center of gravity of the rotorcraft.

In Figure 38, horizontal stabilizer location is illustrated on the flowfield where total air velocity is illustrated by velocity magnitude contours together with vortex particles and streamlines. Wake skew can be seen clearly due to rotor downwash and freestream air velocity. In Figure 39, interactions on case requires higher body pitch angles due to horizontal tail downwash as expected.

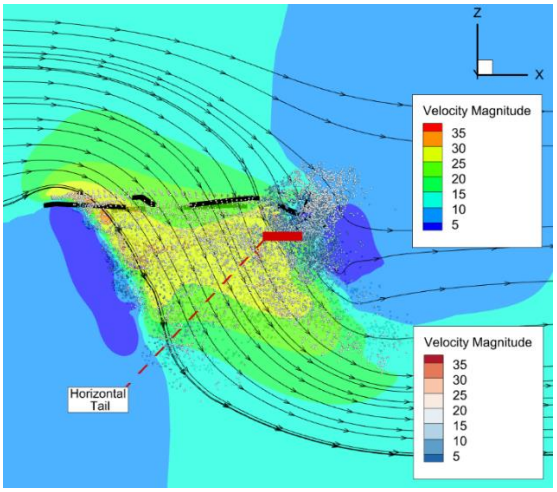

Figure 38 Velocity contours of full helicopter Trim @ 20 knots

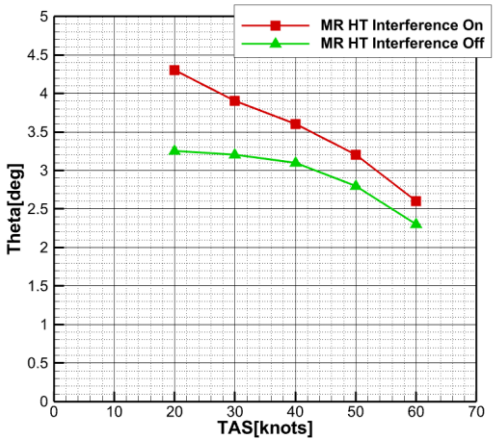

Figure 39 Body Pitch Attitude Interactions On/Off Analysis

7.1.3. Multi-Rotor Full Interaction Simulations

Sample multi-rotor configuration modeled as illustrated in Figure 40. Hover and transition flight trim analyses are performed.

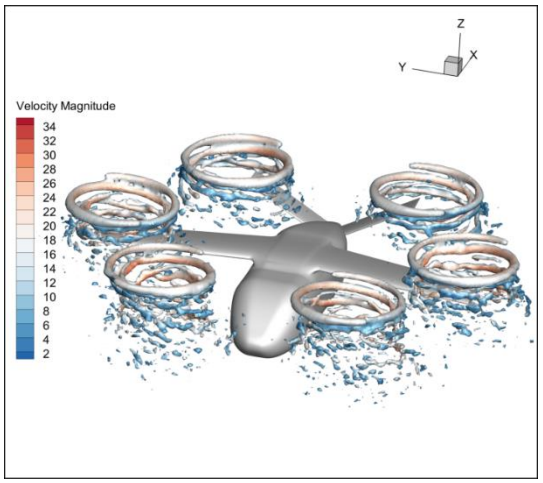

Figure 40 Hover Trim Condition Vorticity Isosurfaces colored by Velocity Magnitude

In Figure 41 and Figure 42, body pitch and roll history of hexacopter configuration is illustrated. Trim is achieved zero pitch and zero roll conditions as expected since the center of gravity is at the center point of rotors.

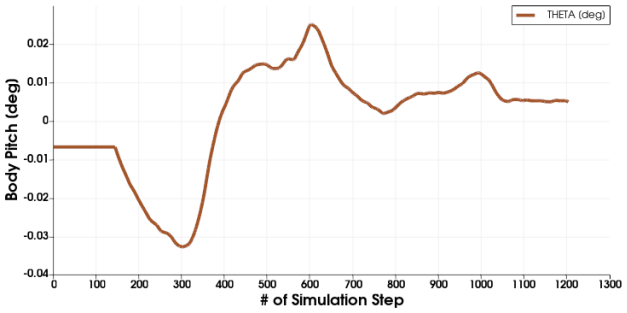

Figure 41 Body pitch angle history for hover trim

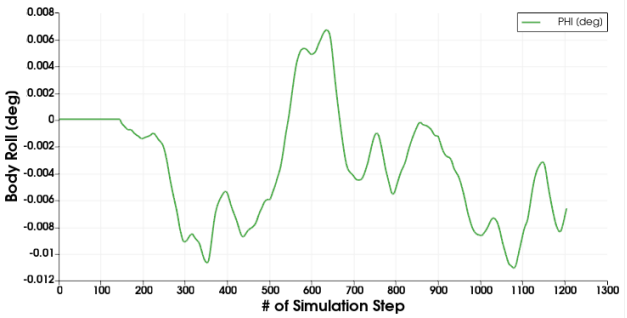

Figure 42 Body roll angle history for hover trim

In Figure 43 and Figure 44 rotor thrust and collective angle input histories of each rotor are provided. After almost 9th revolution, trim point is achieved for hover condition.

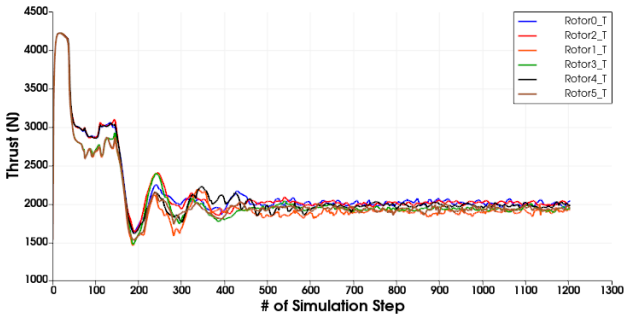

Figure 43 Thrust history for each rotor

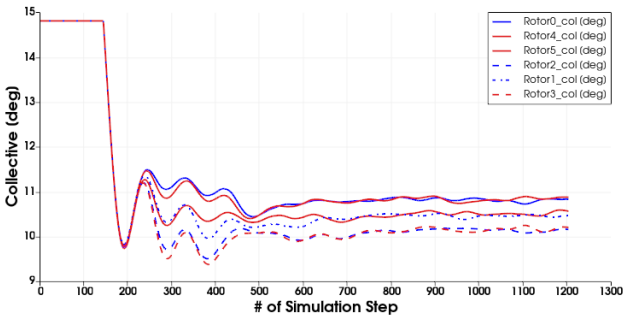

Figure 44 Collective input history for each rotor

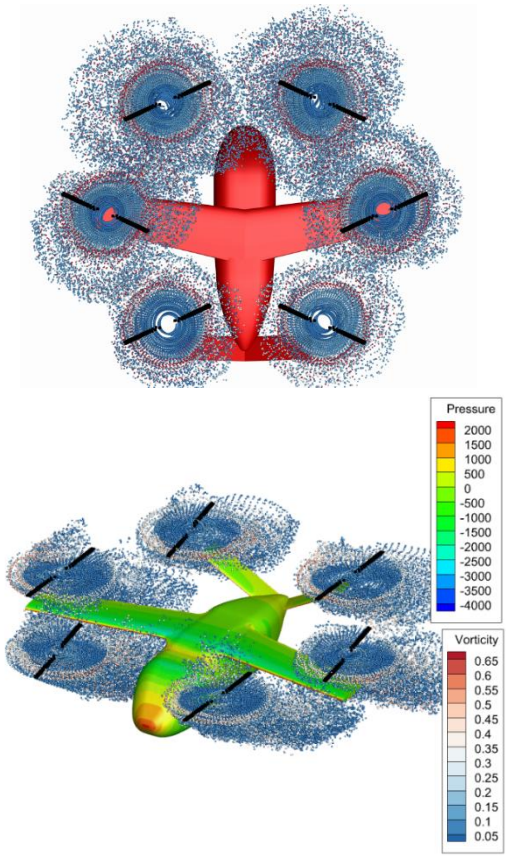

Figure 45 Hover and 10 knots forward flight trim condition vortex particles

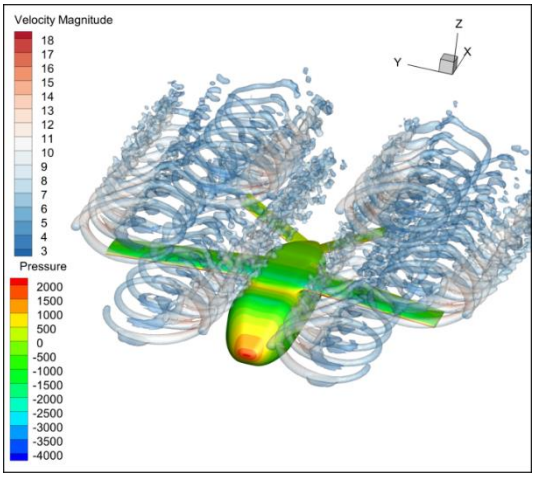

Figure 46 80 knots trim condition Vorticity Isosurfaces colored by Velocity Magnitude

Angle of attack and power values for increasing airspeeds are given in Figure 47 and Figure 48 are provided. Body tilts forward to produce propulsive force and induced power losses are decreases around 40 knots.

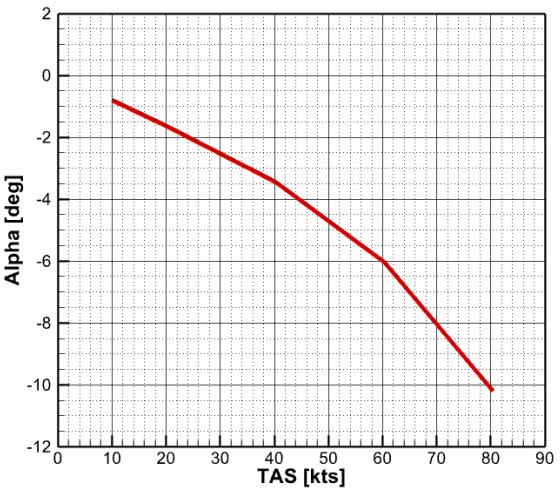

Figure 47 Fuselage α vs. TAS

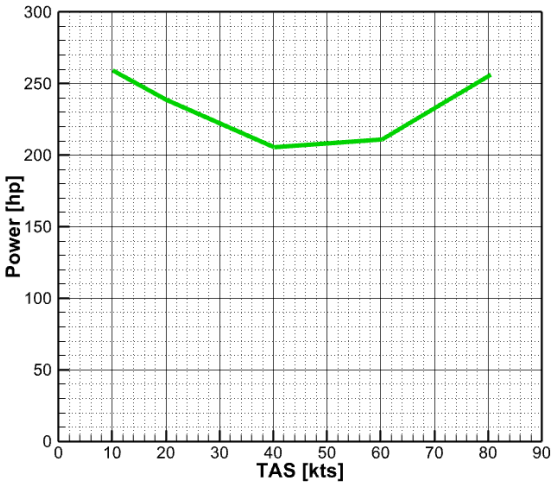

Figure 48 Total required power vs. TAS